Sensors and Actuators B 184 (2013) 235–242

Contents lists available at SciVerse ScienceDirect

Sensors and Actuators B: Chemical

journal homepage: www.elsevier.com/locate/snb

Microchannel plate (MCP) functionalized with Ag nanorods as a high-porosity stable SERS-active membrane

Mengying Zhang, Zhen Cao, Levent Yobas*

Department of Electronic and Computer Engineering, The Hong Kong University of Science and Technology, Clear Water Bay, Kowloon, Hong Kong

ARTICLE INFO

Article history:
Received 5 December 2012
Received in revised form 18 April 2013
Accepted 19 April 2013
Available online 28 April 2013

Keywords:
Ag nanorods
Microchannel plate (MCP)
Localized oblique-angle deposition (LOAD)
Surface-enhanced Raman spectroscopy (SERS)

ABSTRACT

Surface-enhanced Raman scattering (SERS) encountered in interstitial gaps between closely positioned metal nanostructures, hot spots, offers tremendous potential for molecular analysis at the trace or single-molecule level. SERS-active sites, hot spots, can be achieved at a higher density when metal nanostructures are configured on a three-dimensional (3D) platform than on a planar two-dimensional (2D) substrate. Yet, 3D platforms demonstrated thus far such as anodized alumina and microstructured fibers offer capillaries/pores either too narrow for the sample to be infused or may not be compatible with microfluidic integration due to their non-planar feature. Here, we introduce a 3D SERS-active platform based on a planar component that is readily available and presents densely packed highly aligned precision microchannels, the so-called microchannel plate (MCP). The microchannels, owing to their alignment biased at a small but precise angle (7°) with respect to the plate surface normal and their reasonably large diameter (~6 μm) can be functionalized with Ag nanorods through shadowing-based deposition that requires no other template or lithography. The plate functionalized with Ag nanorods delivers an enhancement factor with values in the range of 10^6–10^8 as verified with probing molecules 4-mercatobenzoic acid (4-MBA) and rhodamine-6G.

© 2013 Elsevier B.V. All rights reserved.

1. Introduction

Surface-enhanced Raman scattering (SERS), since its discovery nearly thirty years ago, has taken the center stage because of its tremendous potential for analyzing molecules at the trace or single-molecule level [1–4]. The dramatic enhancement of the vibrational (Raman) spectra from the analyte adsorbed on a roughened metal surface at the nanometer scale has captivated the researchers from the standpoint of understanding the underlying mechanism and devising novel label-free ultrasensitive sensors exploiting the phenomenon. Raman spectroscopy, by probing the vibration modes of individual chemical bonds, reveals molecular "fingerprint" of the analyte without relying on labels. Yet, a broader implementation of such powerful method in applications has been caught up by its extremely small scattering cross section, nearly 14 orders of magnitude lower than a typical fluorescence cross section [5]. This major obstacle could now be overcome with SERS.

For the exact mechanism behind the surface enhancement effect, after much debate, it is now generally accepted that two independent and yet concurrent mechanisms, electromagnetic and chemical effects, play a role, with the former being dominant [2]. Field enhancement, which is highly localized, arises from the excitations of surface plasmons, the collective oscillations of the conduction electrons in a metal surface, couples to and enhances inelastically scattered light (Raman) intensity from the analyte to the quadratic power [6]. The enhancement reaches a remarkable magnitude up to 10^{12} and yet rapidly diminishes with the increased separation between the analyte and the metal surface [7]. The dependence of the overall enhancement on the type of analyte forms the basis for the chemical postulate that attributes the amplification to the resonant intermediate molecular states arising from electronic coupling between the analyte and the metal surface by a charge-transfer mechanism [8]. Many of the experiments to date have been conducted on the nanostructures of the noble metals, particularly Ag and Au, prepared by numerous techniques such as electrochemical roughening through oxidation-reduction cycles (ORC) [3], thin-film islands through vacuum deposition on a flat substrate [9], thin-film nanorods through oblique-angle deposition (OAD) [10], colloidal suspensions of nanoparticles synthesized through reducing metal salts by citrate [11] or borohydride [12] or merely high-power laser ablation of metals in solution [13], ordered arrangement of the nanoparticles through self-assembly [14], and Ag-film over-nanospheres (AgFONs) [15]. In addition to the noble metals, transition metals and semiconductors can also support plasmons and hence SERS [16,17]. These methods are, by and large, tailored toward maximizing the SERS intensity while few are unstable, inherently irreproducible, and unsuitable for large-volume production. The key impediment holding back SERS from analytical

* Corresponding author. Tel.: +852 2358 7068; fax: +852 2358 1485.
E-mail address: eelyobas@ust.hk (L. Yobas).

0925-4005/$ – see front matter © 2013 Elsevier B.V. All rights reserved.
http://dx.doi.org/10.1016/j.snb.2013.04.091

applications is the lack of a robust and facile method of creating deterministic SERS-active substrates that consistently deliver uniform and reproducible enhancement across a massive area. Toward this goal, flat silicon or glass substrates have been fabricated with highly ordered interstices between metal nanostructures via advanced lithography techniques such as electron-beam lithography (EBL) [18], nanosphere lithography (NSL) [19], and nanoimprint lithography (NIL) [20]. However, the limited density of hot spots that can be achieved on a quasi-2D planar surface of such substrates in combination with the limited adsorption kinetics of the analyte that has to diffuse through the stagnant layer of solvent near the surface has kept the enhancement at a modest level ($<10^5$) [21].

Recently, 3D porous structures have been proposed as a template for SERS so as to overcome the articulated challenges of the conventional quasi-2D substrates and further boost the SERS intensity by maximizing the density of hot spots and analyte adsorption within a surface area illuminated by laser [22]. Surface coverage of the analyte also benefits from the reduced diffusion lengths owing to the partitioning of the bulk solution of the analyte into individual pores. Among the 3D porous structures transformed into a SERS-active platform are the anodized layers of silicon [23], GaN [24], and alumina [25–31], track-etched polycarbonate membranes [32], filter papers [33,34], photonic crystal fibers with a hollow or a solid core surrounded by air holes [35–37], and microstructured optical fibers [38,39] and capillaries [40]. To decorate such templates with nanostructures of Au or Ag, various protocols have been implemented leveraging electrochemical deposition methods including immersion plating, and solution-based electroless plating, thermal decomposition, chemical assembly, vacuum infiltration and vapor deposition. Nevertheless, some of these approaches are challenged with the infiltration of metal nanoparticles and/or the surface functionalization deep into high-aspect-ratio pores. Among the anodized substrates, the porous alumina membrane (PAM) has been extensively studied as a SERS template because of its highly regular and densely populated cylindrical nanopores [25–31]. Higher enhancements through PAM are attributed to its optical transparency and waveguiding properties of nanopores that direct the incident beam deeper into the substrate with minimal absorption [25]. Yet, the fairly small diameter of nanopores (up to 400 nm) makes the infiltration of metal particles without the pore clogging a challenge. The same issue also affects the microstructured fibers and capillaries despite the relatively large diameter of their pores (up to few micrometers) as this can be simply negated by their high aspect ratio. Also notable are the SERS templates that are non-porous and yet exhibit a 3D surface topography with pits and microcavities lithographically etched in silicon and then subjected to thin-film Ag or Au vapor deposition [41–43]. More recently, the steep sidewalls of such microcavities have been decorated with SERS-active Ag nanorods through localized oblique-angle deposition (LOAD) [43].

In this study, we introduce a novel SERS-active substrate based on a readily available planar component, namely the microchannel plate (MCP), suitable for the formation of Ag nanorods through LOAD. MCP is a highly porous glass membrane originally developed as an electron multiplier for image intensifiers but also extensively used in particle and photon detectors for a broad spectrum of applications. A typical plate houses millions of precision microchannels highly aligned, densely packed, and often slightly slanted with respect to the surface normal by a small yet precise angle as can be seen in images in Fig. 1a–c [44]. The steep sidewalls of the microchannels readily allow the geometrical shadowing effect to occur in a standard deposition chamber with the plate on a leveled stage and Ag vapor flux arriving at a large oblique incidence angle as schematically described in Fig. 1d. Ag nucleation begins to form on the sidewalls with sites of preferential growth further shadowing the regions behind them. This leads to the growth of distinct Ag nanorods in the direction of deposition on the exposed interiors of the microchannels (Fig. 1e). The plate with a reasonably large pore diameter and pore density combined with the convenience of forming plasmonic nanorods on the exposed sidewalls strikes a balance between surface area for the hot spots and the analyte adsorption and accessibility to the pores for the functionalization and sample loading. Sample analyte can be infused through the plate with relative ease as compared to the earlier 3D SERS templates with fairly small and high aspect ratio pores. With this motivation, we report, for the first time, on the morphology of Ag nanorods formed on MCP and their characteristic SERS activity measured with the probing molecules 4-mercatobenzoic acid (4-MBA) and rhodamine-6G (R6G).

2. Experimental

MCP was obtained from Chairman Photoelectricity S&T Co. Ltd., PR China with straight microchannels at a length of 300 μm (plate thickness) and slanted with respect to the plate surface normal by 7° while terminating at pores 6.25 μm in diameter and $\sim 2.7 \times 10^4$ mm^{-2} in density. The plate was diced into smaller pieces (4 mm × 4 mm). With each piece mounted on a glass slide, LOAD was performed by evaporating Ag either directly on a blank piece or on a layer of sputtered Ag. A base layer of sputtered Ag has been shown to increase SERS intensity by increasing the underlayer reflectivity of Ag nanorods [43,45]. For control, the investigation also included substrates with a sputtered Ag alone. The specimens prepared through distinct Ag deposition methods can be classified into three types: S-type with a sputtered Ag, E-type with an evaporated Ag, and ES-type with an evaporated Ag over a sputtered Ag. The sputtering and evaporation gave rise to a film thickness of 500 nm and 1 μm, respectively. The LOAD process was performed using a pure Ag (99.999% Kurt J Lesker Co.) under vacuum ($<10^{-7}$ Torr) inside a standard electron-beam evaporator (Peva-600EI) with the specimens resting on a leveled stage.

For SERS study, we employed two types of molecules, 4-mercatobenzoic acid (4-MBA, 90%, Sigma–Aldrich) and rhodamine 6G (R6G, 99%, Sigma–Aldrich). 4-MBA was chosen particularly because it is known to form self-assembled monolayer on a metal surface, allowing a reasonably accurate estimation of total amount of surface-adsorbed molecules under Raman irradiation, which, in turn, benefits the accurate calculation of enhancement factor (EF). R6G carries a net positive charge, and can be organized as a second layer on the monolayer of self-assembled 4-MBA in neutral or basic pH, via layer-by-layer electrostatic assembly. It also shows direct and nonspecific adsorption to Ag films, providing a benchmark study between these two distinct surface immobilization approaches. The self-assembled monolayer of 4-MBA was prepared by immersing the fabricated substrates in ethanol solution of 10^{-4} M 4-MBA for ~24 h. The substrates were then rinsed with absolute ethanol and DI water alternately for several times to remove the non-specifically adsorbed molecules. For R6G electrostatic adsorption, substrates were incubated in an aqueous solution of 10^{-4} M R6G for 5 min, followed by copious wash with DI water. This step was repeated three times to ensure adequate nonspecific adsorption of R6G directly on the substrates. Raman spectra were acquired on a Raman microscope (RM3000, Renishaw) equipped with a laser source at a wavelength of 632.8 nm from a cw He/Ne laser (Spectra-Physics/Model 127; I_{max} 60 mW) and of 785 nm from a cw semiconductor diode laser (Renishaw Plc/Model HPNIR785; I_{max} 500 mW) focused directly on the surface pores through a 50× objective (Olympus ULWD). The substrates fabricated were tested either being immersed in ethanol in a quartz cuvette or being exposed to air. SERS spectra were also compared with normal Raman spectra of an ethanol solution of 0.1 M 4-MBA and of

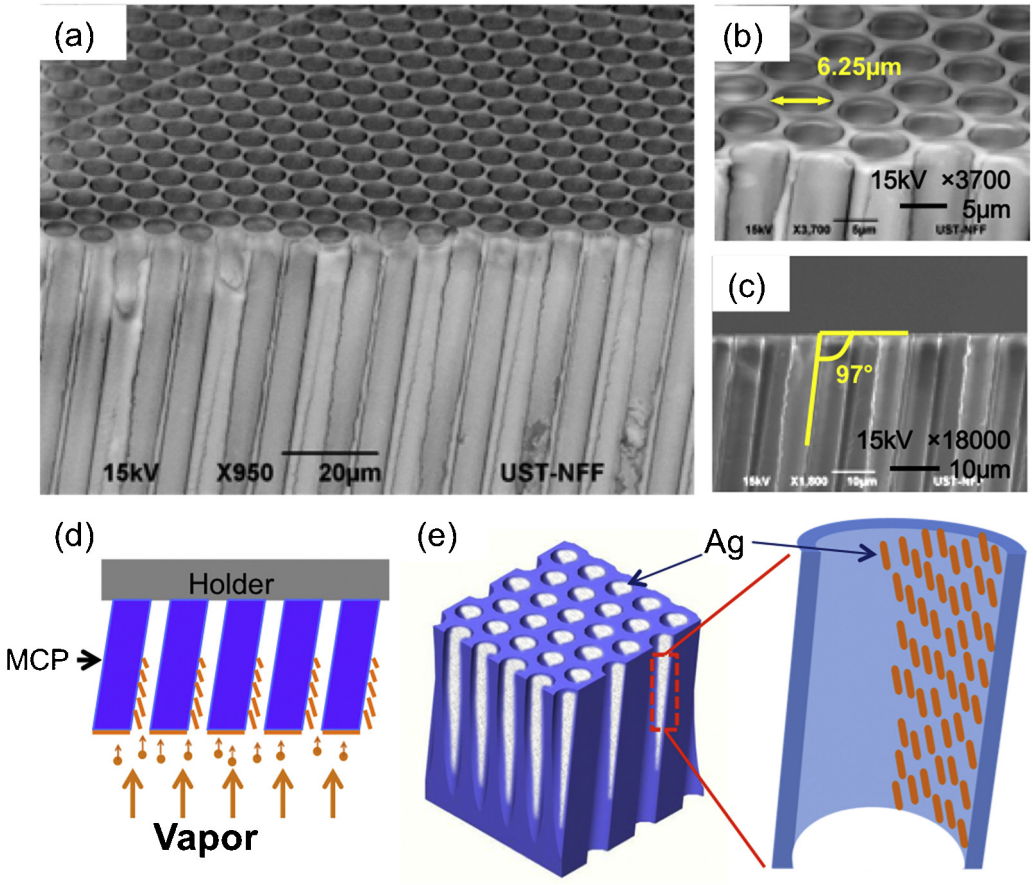

Fig. 1. Scanning electron microscopy (SEM) images from a sectioned microchannel plate (MCP) shown (a and b) in an oblique view and (c) in a cross-sectional view. Illustrations for (d) the localized oblique angle deposition (LOAD) of Ag nanorods as applied on MCP and (e) the projected formation of Ag nanorods on the exposed sections of the steep sidewalls of the slanted microchannels.

an aqueous solution of 0.1 M R6G acquired independently in the presence of blank MCP pieces without Ag.

3. Results and discussion

3.1. Morphology

Fig. 2 reveals morphologies of Ag nanostructures prepared through the distinct deposition methods applied on the substrates. On S-type substrate, due to scattering of the sputtered atoms in all directions, Ag film does not exhibit nanorods but granular nanostructures (Fig. 2a) unlike those on E-type and ES-type substrates. The granular nanostructures range from tens of nanometers to hundreds of nanometers. On the substrates having received 1-μm-thick Ag evaporation, ES-type in Fig. 2b and E-type in Fig. 2c, Ag nanorods are noticeable on the steep sidewalls aligned in the direction of deposition in good homogeneity. Nevertheless, Ag nanorods on ES-type substrate become fused together and could not be individually resolved. The Ag nanorods get deposited exclusively on the exposed interiors of the microchannels and could extend as deep as 45 μm below the surface (Figure SI1 in the Supporting Information). The average diameter and length according to the SEM images are 122.4 ± 21.0 nm ($n = 22$) and 497.2 ± 124.4 nm ($n = 23$), respectively. Meanwhile, E-type substrate, lacking a base layer of sputtered Ag, presents individually resolvable discrete Ag nanorods, with an average diameter of 95.7 ± 17.9 nm ($n = 32$) and a length of 560.3 ± 121.8 nm ($n = 33$). The calculated aspect ratio of the nanorods is accordingly 4.06 for ES-type while 5.85 for E-type substrates. Based on the investigation of morphologies, we conclude that (1) Ag evaporation on these substrates gives rise to nanorods, while sputtering produces only granular nanostructures; (2) nanorods tend to aggregate and fuse together when evaporated on a base layer of sputtered Ag; (3) while those evaporated on a blank substrate become more discrete and individually isolated, thus offering a higher aspect ratio.

Supplementary data associated with this article can be found, in the online version, at http://dx.doi.org/10.1016/j.snb.2013.04.091.

3.2. SERS measurements

E-type substrate, with individually resolved Ag nanorods, is likely to show a strong SERS effect. Raman spectra obtained with the excitation wavelengths at 632.8 nm and 785 nm on blank (MCP without metal film) and E-type substrates are compared in Fig. 3. Traces I and II, respectively, refer to the spectrum of absolute ethanol and ethanol solution of 0.1 M 4-MBA in the presence of a blank substrate, while trace III corresponds to a monolayer of 4-MBA self-assembled on E-type substrate. The small but noticeable peak in trace II (arrow) is not present in trace I and coincides with a Raman band of a 4-MBA molecule (at 1596 cm^{-1}). The peak, although it is quite weak in Fig. 3b, is still detectable through peak analysis software. The peak gets highly intensified in the spectrum of a 4-MBA monolayer on E-type substrate (trace III) along with some other peaks barely noticeable in trace II. Such highly enhanced peaks testify that Ag nanorods on E-type substrate can boost normal Raman signal of 4-MBA molecules.

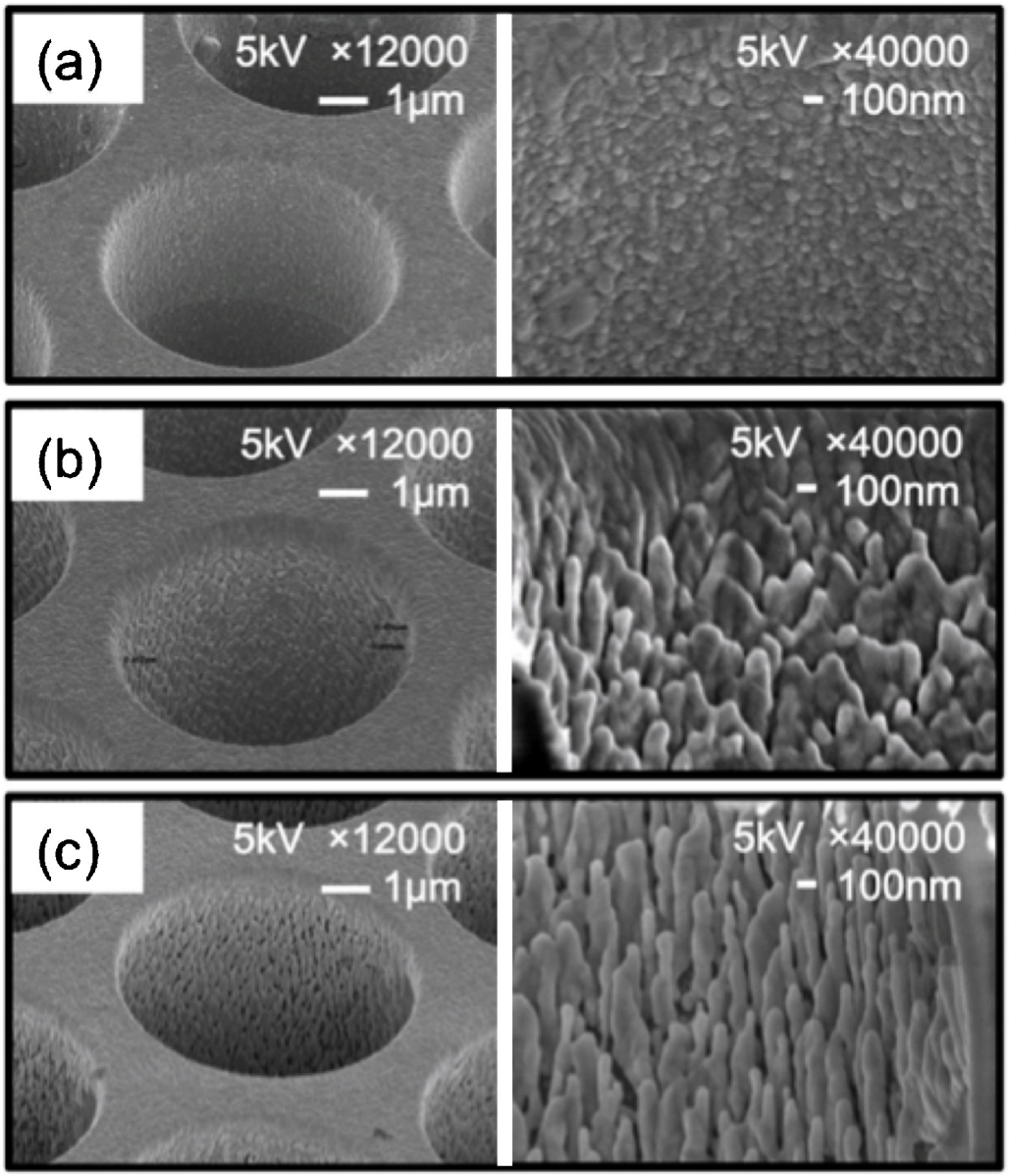

Fig. 2. SEM images of representative microchannel pores from MCP specimens deposited with Ag nanostructures. Oblique views (left) and cross-sectional views after Ag deposition by (a) sputtering alone (S-type), (b) evaporation over sputtering (ES-type) and (c) evaporation alone (E-type).

Having a monolayer of 4-MBA assembled on Ag, the peak slightly shifts from 1596 cm^{-1} to 1584 cm^{-1} and, together with another band at 1077 cm^{-1}, forms one of the two characteristic bands that belong to ν(C–C) ring-breathing mode [46]. The peak at 1584 cm^{-1} displays a higher relative intensity than the one at 1077 cm^{-1} when obtained with 632.8 nm excitation but the order is reversed with 785 nm excitation. Though both bands can be considered for the evaluation of enhancement factor (EF), the band at 1584 cm^{-1} is preferred here as it can be identified in normal Raman spectrum (trace II) and less interfered by solvent bands.

All the three types of substrates, expressing a distinct morphology of nanostructures, are evaluated for SERS activity by analyzing the spectra of the self-assembled monolayer of 4-MBA. Fig. 4 reveals the spectra acquired with an excitation wavelengths at 632.8 and 785 nm probing the substrates either in ethanol (Fig. 4a) or while being exposed to air (Fig. 4b). Traces a, b and c refer to the spectra obtained with substrates S-type, ES-type and E-type, respectively. Raman shifts found at 523, 715, 840, 1077, 1139, 1184, 1372, 1481 and 1584 cm^{-1} all agree well with the earlier reports of 4-MBA molecules [46–49]. With respect to their SERS activity, the substrates can be ranked in descending order as E-type (trace c), ES-type (trace b), and S-type (trace a). The peaks acquired with the substrates exposed to air (Fig. 4b) are found at a much greater intensity than those obtained with the substrates immersed in ethanol (Fig. 4a). Among the three, E-type substrate stands out offering much stronger SERS enhancement.

3.3. Enhancement factors

To quantify the degree of SERS activity in the fabricated substrates, surface enhancement factor (EF) for each substrate is calculated for a specified band by comparing the experimentally measured SERS intensity and normal Raman intensity according to the following expression [50]:

$$\mathrm{EF} = \frac{N_R I_{\mathrm{SERS}}}{N_{\mathrm{SERS}} I_R} \quad (1)$$

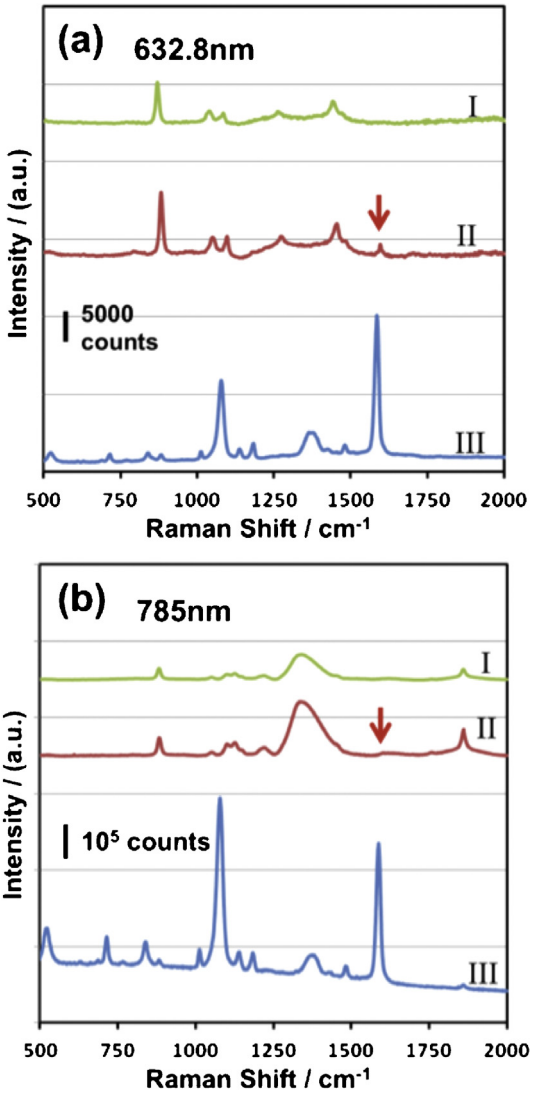

Fig. 3. Raman spectra of absolute ethanol (trace I) and an ethanol solution of 0.1 M 4-MBA (trace II) both in the presence of a blank substrate (MCP without metal film). SERS spectrum of a monolayer of 4-MBA assembled on E-type substrate immersed in ethanol (trace III). (a) Acquired with 632.8 nm excitation 7.05 mW laser power with traces I and III each accumulated 1 spectrum while trace II 10 spectra. (b) Acquired with 785 nm excitation 152 mW laser power with traces I, II and III accumulated 2, 10 and 1 spectra, respectively. Integration time: 10 s. Arrows in trace II: the peak that corresponds to a Raman band of a 4-MBA molecule at 1584 cm^{-1}.

where N_{SERS} and N_R are the total number of molecules absorbed on the surface of the nanostructures and in a bulk reference solution subjected to the laser illumination, respectively. The total number of molecules are calculated based on the following assumptions and measurements: (1) the size of a single 4-MBA molecule is 0.64 nm in accordance with the maximum van der Waals diameter along the phenyl ring [51]; (2) a monolayer of 4-MBA molecules tightly packed entirely covers microchannel area irradiated under a laser spot of a diameter 1 μm during 632.8 nm excitation and a laser spot of 2 μm × 24 μm during 785 nm excitation; (3) effective focal depth for either excitation is 15.7 and 17.9 μm, respectively. In our experimental setting, this effective focal depth was estimated by focusing the laser beam on a polished surface of a single crystal silicon and then gradually overfocusing into the crystal to identify the depth at which the intensity of 520 cm^{-1} Si band is reduced to 50% of its original value at the crystal surface [49]. Thus, the effective focal volume of bulk solution for 632.8 and 785 nm excitation is calculated to be 2317 and 8989 μm^3, respectively. Knowing the effective focal volume and the concentration of solution, one may calculate N_R as 1.4×10^{11} and 5.4×10^{11} molecules in the reference solution subjected to 632.8 and 785 nm excitation, respectively. Based on the estimated surface area, N_{SERS} can be calculated as 9.8×10^6 and 1.5×10^8 for the specified wavelengths, respectively.

Table 1 lists the EF values calculated with respect to the band at 1584 cm^{-1} in the spectra of a monolayer of 4-MBA assembled on the substrates. E-type substrate manifests the highest SERS effect with EF approaching 10^8 among those probed in air with 632.8 nm excitation. It shows a substantial boost in EF surpassing the other two types of substrate by at least several folds if not an order of magnitude. Among those immersed in ethanol during the same excitation wavelength (632.8 nm), E-type returns enhancement twice as much as ES-type while nearly four times as much as S-type. E-type exceeds S-type by an order of magnitude when they were probed with 785 nm excitation.

Fig. 5 compares SERS spectra of non-specifically adsorbed R6G and electrostatically adsorbed (sub)monolayer of R6G on a monolayer of self-assembled 4-MBA, all acquired on E-type substrate at 632.8 nm excitation. In spectrum (a), characteristic bands of R6G molecules can be identified as 612, 772, 1080, 1183, 1311, 1362, 1510, 1578 and 1650 cm^{-1}, concurring with earlier reports [52,53]. The peak positions among the three spectra confirm that trace in (b) R6G-4-MBA double layer is a superposition of those independently acquired in (a) R6G and (c) 4-MBA. Both the peak positions and the relative intensities of R6G in spectra (a) and (b) are comparable, suggesting that R6G molecules are retained well both when electrostatically adsorbed on a 'soft' layer of 4-MBA and when adsorbed non-specifically on 'hard' Ag film with nanorods.

SERS spectra of a non-specifically adsorbed layer of R6G and an electrostatic double layer of R6G-4MBA have also been acquired on both S-type and ES-type substrates (not shown). Two stable R6G bands identified as 612 cm^{-1} and 1510 cm^{-1} are employed in the calculation of EF as both bands are at a relatively strong intensity and well isolated from the bands of 4-MBA. N_{SERS} is estimated to be 8.1×10^5 based on the size of a single R6G molecule 1.6 nm × 1.1 nm [54]. Table 2 lists EFs calculated at 632.8 nm excitation for all the three substrate types with R6G adsorbed either nonspecifically on a 'hard' Ag or electrostatically on a 'soft' 4-MBA monolayer. Typically, the configuration of the electrostatic double layer (R6G-4MBA) shows a higher SERS effect than that of the non-specifically adsorbed layer. In either case, E-type substrate returns the highest value with EF typically in the orders of 10^7 overtaking those from ES-type and S-type. Often, the SERS effect favors the band at 612 over 1510 cm^{-1}.

We compared the results obtained here to those of our previous study where we had the technique (LOAD) performed on microstructured Si substrates and with Ag nanorods deposited on the sidewalls of Si microcavities [43]. Due to the isotropic etched parabolic profile of those microcavities, the incidence angle of deposition was not uniform but spatially varied along the profile, gradually diminishing toward the center of the microcavities from a maximum angle 83.6° at the very edge. In contrast, the precisely aligned microchannels here, with a mirror-finish surface that is free of etched roughness, pose a large incidence angle of 83° fixed spatially uniform throughout the pore depth and allow the formation of reasonably well-defined Ag nanorods along the exposed sidewalls. For a fair comparison, Ag nanorods deposited on such Si microcavities were assembled here with a monolayer of 4-MBA molecules adhering to the same experimental procedure and then probed for SERS effect. Maximum EFs based on the spectra acquired (not shown) with the substrates exposed to air or immersed in ethanol are 1.1×10^7 and 1.3×10^6, respectively. These values are an order of magnitude lower than those obtained with the E-type substrate configuration of MCP.

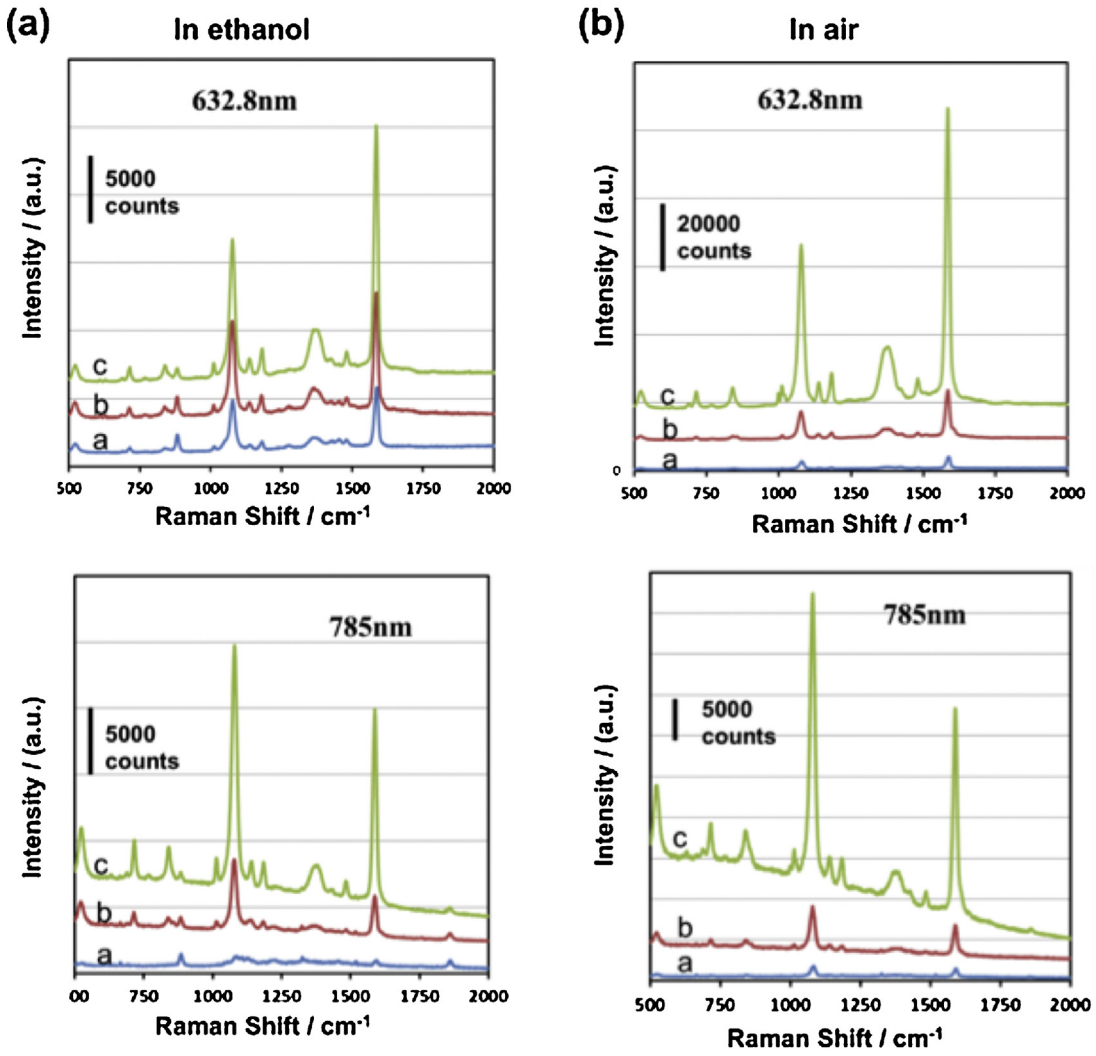

Fig. 4. SERS spectra of a monolayer of 4-MBA self-assembled on S-type (trace a), ES-type (trace b) and E-type (trace c) substrates (a) probed in the presence of absolute ethanol or (b) while being exposed to air. Spectra were acquired with the excitation wavelength at 632.8 and 785 nm and the laser power, respectively, at (a) 7.05 and 6.12 mW, and (b) 0.8 and 0.9 mW. Integration time: 10 s.

Table 1
Calculated EF values for the Raman shift of 4-MBA at 1584 cm^{-1}.

Wavelength (nm)	EF values ($\times 10^6$) and the substrate types (S, ES, and E)					
	In ethanol			In air		
	S	ES	E	S	ES	E
632.8	0.6	1.1	2.3	3.7	14.3	94.4
785	0.04	0.4	1.9	0.8	3.1	21.8

We believe that the SERS response of such nanorods here could be further optimized. It has been previously reported that the length, diameter, and density of the Ag nanorods have direct influence on the SERS response along with the excitation configuration such as the incident angle and the polarization of the excitation light [55]. The diameter and the density of the Ag nanorods are typically varied with the nanorod length and deposition angle. The deposition angle here, however, is fixed at 83° by the biased

Table 2
Calculated EF values from the spectra of non-specifically adsorbed R6G and electrostatically adsorbed (sub)monolayer of R6G on a monolayer of self-assembled 4-MBA both acquired with 632.8 nm excitation.

Peak position (cm^{-1})	EF values ($\times 10^6$) and the substrate types (S, ES, and E)					
	R6G			R6G on 4-MBA		
	S	ES	E	S	ES	E
612	0.03	7.1	15.6	1.0	1.8	40.8
1510	0.002	0.8	1.8	0.09	1.8	29.2

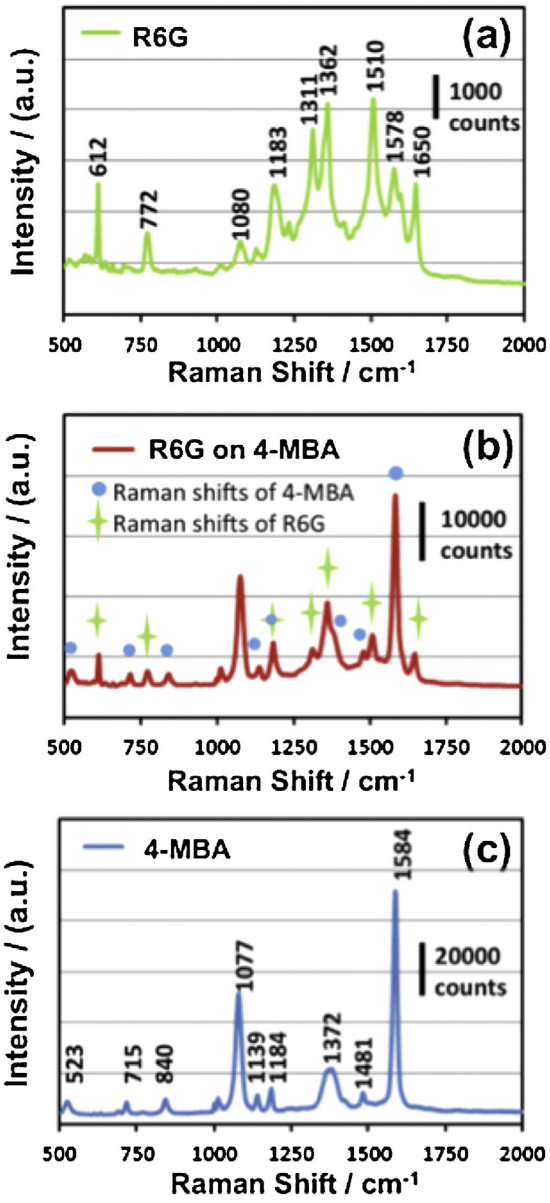

Fig. 5. SERS spectra acquired on E-type substrate with 632.8 nm excitation at 7.05 mW: (a) non-specifically and directly adsorbed R6G, (b) electrostatically adsorbed (sub)monolayer of R6G on a monolayer of self-assembled 4-MBA, and (c) a monolayer of self-assembled 4-MBA. Four spectra accumulated in (a) while one spectrum in (b) and (c). Integration: 10 s.

alignment of the microchannels which left us with the deposition length as the tuning parameter. The average diameter of ~96 nm obtained at a length of ~560 nm on E-type substrates appears ideal given that an optimum SERS activity of the Ag nanoparticles is obtained with the nanoparticles at a critical size of about 100 nm as reported by Mo et al. [56] and Du et al. [57]. Liu et al. [55] validated this critical size for the Ag nanorods fabricated at a deposition angle of 84°. All these point to the excitation configuration as a possible source of future enhancements to the SERS response, which needs to be further investigated.

4. Conclusions

We introduce an effective SERS-active substrate based on the readily available high porosity precision glass membrane decorated with Ag nanorods through a method of simple shadow-based deposition. Preparation of the substrate for SERS use does not demand sophisticated cleanroom processes but a standard evaporation chamber, owing to the oblique and precise arrangement of uniform microchannels, an ideal template for LOAD. Quality SERS spectra were obtained from the substrates prepared with a monolayer of self-assembled 4-MBA, an electrostatic double layer of R6G-4-MBA and a layer of R6G nonspecifically and directly adsorbed. Provided that Ag evaporation takes place on a blank substrate without a base film of sputtered Ag, the EF values range from 10^6 to 10^8 on par with or better than those acquired on the substrates demanding more involved preparation. With the material bulk in glass and the configuration planar, the new type of SERS-active substrate can be readily integrated in microfluidics for an automated sample delivery or for an in-line analysis of trace elements. Partitioning the sample flow into millions of identical microchannels with each <10 μm in diameter would therefore minimize the diffusion length that the target analyte must overcome to reach hot spots on the sidewalls, enabling a fast and effective detection.

Acknowledgements

This project was financially supported in part by the Startup Grant from the ECE Department, HKUST, the Research Project Competition Grant by the HKUST (Grant No. RPC11EG09) and the Research Grant Council of Hong Kong, a Direct Allocation Grant to HKUST (Grant No. DAG09/10.EG09).

References

[1] D.L. Jeanmaire, R.P. Van Duyne, Surface Raman spectroelectrochemistry: Part I. Heterocyclic, aromatic, and aliphatic amines adsorbed on the anodized silver electrode, Journal of Electroanalytical Chemistry 84 (1977) 1–20.
[2] M. Moskovits, Surface-enhanced spectroscopy, Review of Modern Physics 57 (1985) 783–826.
[3] M. Fleischmann, P. Hendra, A. McMillan, Raman spectra of pyridine adsorbed at a silver electrode, Chemical Physical Letters 26 (1974) 163–166.
[4] M. Fleischmann, P.J. Hendra, A.J. McQuillan, Raman spectra from electrode surface, Journal of the Chemical Society Chemical Communications 3 (1973) 80–81.
[5] R.L. McCreery, Raman Spectroscopy for Chemical Analysis, John Wiley & Sons, New York, 2000.
[6] W. Knoll, Interfaces and thin films as seen by bound electromagnetic waves, Annual Review of Physical Chemistry 49 (1998) 569–638.
[7] M. Moskovits, D.P. DiLella, K. Maynard, Surface Raman spectroscopy of a number of cyclic aromatic molecules adsorbed on silver: selection rules and molecular reorientation, Langmuir 4 (1988) 67–76.
[8] A. Campion, J.E. Ivanecky III, C.M. Child, M.C. Foster, On the mechanism of chemical enhancement in surface-enhanced Raman scattering, Journal of the American Chemical Society 117 (1995) 11807–11808.
[9] V.L. Schlegel, T.M. Cotton, Silver-island films as substrates for enhanced Raman scattering: effect of deposition rate on intensity, Analytical Chemistry 63 (1991) 241–247.
[10] S.B. Chaney, S. Shanmukh, R.A. Dluhy, Y.P. Zhao, Aligned silver nanorod arrays produce high sensitivity surface-enhanced Raman spectroscopy substrates, Applied Physics Letters 87 (2005) 031908.
[11] L. Rivas, S. Sanchez-Cortes, J.V. Garcia-Ramos, G. Morcillo, Growth of silver colloidal particles obtained by citrate reduction to increase the Raman enhancement factor, Langmuir 17 (2001) 574–577.
[12] M. Muniz-Miranda, SERS-active Ag/SiO_2 colloids: photoreduction mechanism of the silver ions and catalytic activity of the colloidal nanoparticles, Journal of Raman Spectroscopy 35 (2004) 839–842.
[13] J. Neddersen, G. Chumanov, T.M. Cotton, Laser ablation of metals: a new method for preparing SERS active colloids, Applied Spectroscopy 47 (1993) 1959.
[14] S. Lin, M. Li, E. Dujardin, C. Girard, S. Mann, One-dimensional plasmon coupling by facile self-assembly of gold nanoparticles into branched chain networks, Advanced Materials 17 (2005) 2553–2559.
[15] C.L. Haynes, C.R. Yonzon, X. Zhang, R.P. vanDuyne, Surface-enhanced Raman sensors: early history and the development of sensors for quantitative biowarfare agent and glucose detection, Journal of Raman Spectroscopy 36 (2005) 471–484.
[16] Z.Q. Tian, B. Ren, D.Y. Wu, Surface-enhanced Raman scattering: from noble to transition metals and from rough surfaces to ordered nanostructures, Journal of Physical Chemistry B 106 (2002) 9463–9483.
[17] Y.F. Wang, Z.H. Sun, H.L. Hu, S.Y. Jing, B. Zhao, W.Q. Xu, C. Zhao, J.R. Lombardi, Raman scattering study of molecules adsorbed on ZnS nanocrystals, Journal of Raman Spectroscopy 38 (2007) 34–38.

[18] M. Kahl, E. Voges, S. Kostrewa, C. Viets, W. Hill, Periodically structured metallic substrates for SERS, Sensors and Actuators B 51 (1998) 285–291.
[19] J.C. Hulteen, D.A. Treichel, M.T. Smith, M.L. Duval, T.R. Jensen, R.P. Van Duyne, Nanosphere lithography: size-tunable silver nanoparticle and surface cluster arrays, Journal of Physical Chemistry B 103 (1999) 3854–3863.
[20] R. Alvarez-Puebla, B. Cui, J.-P. Bravo-Vasquez, T. Veres, H. Fenniri, Nanoimprinted SERS-active substrates with tunable surface plasmon resonances, Journal of Physical Chemistry C 111 (2007) 6720–6723.
[21] M.J. Natan, Concluding remarks surface enhanced Raman scattering, Faraday Discussions 132 (2006) 321–328.
[22] H. Ko, S. Singamaneni, V.V. Tsukruk, Nanostructured surfaces and assemblies as SERS media, Small 4 (2008) 1576–1599.
[23] S. Chan, S. Kwon, T.W. Koo, L.P. Lee, A.A. Berlin, Surface-enhanced Raman scattering of small molecules from silver-coated silicon nanopores, Advanced Materials 15 (2003) 1595–1598.
[24] T.L. Williamson, X. Guo, A. Zukoski, A. Sood, D.J. Diaz, P.W. Bohn, Porous GaN as a template to produce surface-enhanced raman scattering-active surfaces, Journal of Physical Chemistry B 109 (2005) 20186–20191.
[25] R.J. Walsh, G. Chumanov, Silver coated porous alumina as a new substrate for surface-enhanced Raman scattering, Applied Spectroscopy 55 (2001) 1695–1700.
[26] H. Ko, V.V. Tsukruk, Nanoparticle-decorated nanocanals for surface-enhanced Raman scattering, Small 4 (2008) 1980–1984.
[27] H. Ko, S. Chang, V.V. Tsukruk, Porous substrates for label-free molecular level detection of nonresonant organic molecules, Nano 3 (2009) 181–188.
[28] Z. Lu, W. Ruan, J. Yang, W. Xu, C. Zhao, B. Zhao, Deposition of Ag nanoparticles on porous anodic alumina for surface enhanced Raman scattering substrate, Journal of Raman Spectroscopy 40 (2009) 112–116.
[29] S. Chang, Z.A. Combs, M.K. Gupta, R. Davis, V.V. Tsukruk, In situ growth of silver nanoparticles in porous membranes for surface-enhanced Raman scattering, Applied Materials and Interfaces 2 (2010) 3333–3339.
[30] R. Kodiyath, T.A. Papadopoulos, J. Wang, Z.A. Combs, H. Li, R.J.C. Brown, J.-L. Brédas, V.V. Tsukruk, Silver-decorated cylindrical nanopores: combining the third dimension with chemical enhancement for efficient trace chemical detection with SERS, Journal of Physical Chemistry C 116 (2012) 13917–13927.
[31] X. Wang, S. Xu, H. Li, J. Tao, B. Zhao, W. Xu, A three-dimensional surface-enhanced Raman scattering substrate: Au nanoparticle supramolecular self-assembly in anodic aluminum oxide template, Journal of Raman Spectroscopy 43 (2012) 459–463.
[32] K.R. Wigginton, P.J. Vikesland, Gold-coated polycarbonate membrane filter for pathogen concentration and SERS-based detection, Analyst 135 (2010) 1320–1326.
[33] M.-L. Cheng, B.-C. Tsai, J. Yang, Silver nanoparticle-treated filter paper as a highly sensitive surface-enhanced Raman scattering (SERS) substrate for detection of tyrosine in aqueous solution, Analytica Chimica Acta 708 (2011) 89–96.
[34] C.D. Tran, Subnanogram detection of dyes on filter paper by surface-enhanced Raman scattering spectrometry, Analytical Chemistry 56 (1984) 824–826.
[35] X. Yang, C. Shi, D. Wheeler, R. Newhouse, B. Chen, J.Z. Zhang, C. Gu, High-sensitivity molecular sensing using hollow-core photonic crystal fiber and surface-enhanced Raman scattering, Journal of Optical Society of America A 27 (2010) 977–984.
[36] M.K. Khaing Oo, Y. Han, J. Kanka, S. Sukhishvili, H. Du, Structure fits the purpose: photonic crystal fibers for evanescent-field surface-enhanced Raman spectroscopy, Optical Letters 35 (2010) 466–468.
[37] Y. Han, S. Tan, M.K. Khaing Oo, D. Pristinski, S. Sukhishvili, H. Du, Towards full-length accumulative surface-enhanced Raman scattering-active photonic crystal fibers, Advanced Materials 22 (2010) 2647–2651.
[38] A. Amezcua-Correa, J. Yang, C.E. Finlayson, A.C. Peacock, J.R. Hayes, P.J.A. Sazio, J.J. Baumberg, S.M. Howdle, Surface-enhanced Raman scattering using microstructured optical fiber substrates, Advanced Functional Materials 17 (2007) 2024–2030.
[39] F.M. Cox, A. Argyros, M.C.J. Large, S. Kalluri, Surface-enhanced Raman scattering in a hollow core microstructured optical fiber, Optics Express 15 (2007) 13675–13681.
[40] Y. Guo, M.K.K. Oo, K. Reddy, X. Fan, Ultrasensitive optofluidic surface-enhanced Raman scattering detection with flow-through multihole capillaries, Nano 6 (2012) 381–388.
[41] K.C. Vernon, T.J. Davis, F.H. Scholes, D.E. Gomez, D. Lau, Physical mechanisms behind the SERS enhancement of pyramidal pit substrates, Journal of Raman Spectroscopy 41 (2010) 1106–1111.
[42] T.A. Alexander, D.M. Le, Characterization of a commercialized SERS-active substrate and its application to the identification of intact Bacillus endospores, Applied Optics 46 (2007) 3878–3890.
[43] J. Fu, Z. Cao, L. Yobas, Localized oblique-angle deposition: Ag nanorods on microstructured surfaces and their SERS characteristics, Nanotechnology 22 (2011) 505302.
[44] J.L. Wiza, Microchannel plate detectors, Nuclear Instruments Methods 162 (1979) 587–601.
[45] Q. Zhou, Y.J. Liu, Y.P. He, Z.J. Zhang, Y.P. Zhao, The effect of underlayer thin films on the surface-enhanced Raman scattering response of Ag nanorod substrates, Applied Physics Letters 97 (2010) 121902.
[46] C.J. Orendorff, A. Gole, T.K. Sau, C.J. Murphy, Surface-enhanced Raman spectroscopy of self-assembled monolayers: sandwich architecture and nanoparticle shape dependence, Analytical Chemistry 77 (2005) 3261–3266.
[47] P.N. Sisco, C.J. Murphy, Surface-coverage dependence of surface-enhanced raman scattering from gold nanocubes on self-assembled monolayers of analyte, Journal of Physical Chemistry A 113 (2009) 3973–3978.
[48] C.E. Talley, L. Jusinski, C.W. Hollars, S.M. Lane, T. Huser, Intracellular pH sensors based on surface-enhanced Raman scattering, Analytical Chemistry 76 (2004) 7064–7068.
[49] Y. Li, H. Su, K.S. Wong, X.Y. Li, Surface-enhanced raman spectroscopy on two-dimensional networks of gold nanoparticle-nanocavity dual structures supported on dielectric nanosieves, Journal of Physical Chemistry C 114 (2010) 10463–10477.
[50] A.D. McFarland, M.A. Young, J.A. Dieringer, R.P. Van Duyne, Wavelength-scanned surface-enhanced Raman excitation spectroscopy, Journal of Physical Chemistry B 109 (2005) 11279–11285.
[51] J.R.I. Lee, T.M. Willey, J. Nilsson, L.J. Terminello, J.J. De Yoreo, T. van Buuren, Effect of ring substitution position on the structural conformation of mercaptobenzoic acid self-assembled monolayers on Au(1 1 1), Langmuir 22 (2006) 11134–11141.
[52] H. Liu, L. Zhang, X. Lang, Y. Yamaguchi, H. Iwasaki, Y. Inouye, Q. Xue, M. Chen, Single molecule detection from a large-scale SERS-active $Au_{79}Ag_{21}$ substrate, Scientific Reports 1 (2011) 1–5.
[53] H. Watanabe, N. Hayazawa, Y. Inouye, S. Kawata, DFT vibrational calculations of Rhodamine 6G adsorbed on silver: analysis of tip-enhanced Raman spectroscopy, Journal of Physical Chemistry B 109 (2005) 5012–5020.
[54] L.A. Philips, S.P. Webb, J.H. Clark, High-pressure studies of rotational reorientation dynamics—the role of dielectric friction, Journal of Chemical Physics 83 (1985) 5810–5821.
[55] Y.-J. Liu, H.Y. Chu, Y.-P. Zhao, Silver nanorod array substrates fabricated by oblique angle deposition: morphological, optical, and SERS characterizations, Journal of Physical Chemistry C 114 (2010) 8176–8183.
[56] Y. Mo, I. Mörke, P. Wachter, The influence of surface roughness on the Raman scattering of pyridine on copper and silver surfaces, Solid State Communications 50 (1984) 829–832.
[57] Y. Du, L. Shi, T. He, X. Sun, Y. Mo, SERS enhancement dependence on the diameter and aspect ratio of silver-nanowire array fabricated by anodic aluminium oxide template, Applied Surface Science 255 (2008) 1901–1905.

Biographies

Mengying Zhang received the B.S. degree in applied physics from The University of Science and Technology of China, Chengdu, China, in 2006 and the Ph.D. degree in nanoscience and nanotechnology from The Hong Kong University of Science and Technology (HKUST), Kowloon, Hong Kong, in 2011. She was a research associate with the Department of Electronic and Computer Engineering, HKUST. Her research interests are in microfluidics and droplet-based lab-on-a-chip technologies.

Zhen Cao received the B.S. degree in microelectronics from Fudan University, Shanghai, China. He is currently working toward the Ph.D. degree in the Department of Electronic and Computer Engineering, The Hong Kong University of Science and Technology, Kowloon, Hong Kong. His research interests primarily include silicon-based micro/nanofabrication, electrokinetic-based separation and enrichment methods, biomicrofluidics, and lab-on-a-chip systems for biomedical applications.

Levent Yobas received the B.S. degree in electrical engineering from Hacettepe University, Ankara, Turkey, and the M.S. and Ph.D. degrees both in biomedical engineering from Case Western Reserve University, Cleveland, OH. He was with the BioMEMS Group, Standard MEMS, Inc., Southbridge and Burlington, MA, developing MEMS for drug screening technologies. From 2002 to 2010, he was with the Institute of Microelectronics, Agency for Science, Technology, and Research (A*STAR), Singapore, where he was a senior research engineer and then a Member of the Technical Staff in MEMS, BioMEMS, and bioelectronics. He also held adjunct faculty positions with the Bioengineering Division, National University of Singapore, and the School of Electrical and Electronic Engineering, Nanyang Technological University. He is currently with the Department of Electronic and Computer Engineering and the Division of Biomedical Engineering, The Hong Kong University of Science and Technology, Kowloon, Hong Kong. He has mainly published in the areas of nucleic acid analysis, patch clamp electrophysiology, and droplet microfluidics. His earlier work dealt with integrated electrostatic microvalves for a MEMS-based low-cost low-power refreshable Braille display system. His research is mainly focused on silicon-based micro/nanofabrication technologies for life sciences, drug discovery, and point-of-care diagnostics.